NASA Technical Memorandum 107173

Design and Analysis of Transitions From Rectangular Waveguide to Layered Ridge Dielectric Waveguide

George E. Ponchak
Lewis Research Center
Cleveland, Ohio

Nihad I. Dib
Jordan University of Science and Technology
Jordan

and

Linda P. B. Katehi
University of Michigan
Ann Arbor, Michigan

March 1996

National Aeronautics and
Space Administration

Design and Analysis of Transitions from Rectangular Waveguide to Layered Ridge Dielectric Waveguide

George E. Ponchak, Nihad I. Dib, and Linda P. B. Katehi

February 6, 1996

ABSTRACT

Transitions from rectangular waveguide to layered ridge dielectric waveguide are studied both experimentally and theoretically. In addition, a design procedure is given for each transition. The analysis and design procedures are valid for transitions between rectangular waveguide and other open dielectric waveguides such as Image Guide, Insulated Image Guide, Dielectric Ridge Guide, and Inverted Strip Dielectric Waveguide. It is shown that for small dielectric waveguides such as Layered Ridge Dielectric Waveguide, a transition which is comprised of a tapered ridge waveguide reduces the radiation loss by at least 1 dB.

I. Introduction

There has been a growing interest in the millimeter wave frequency spectrum for aircraft ground avoidance radars, intelligent vehicle highway systems, space debris tracking, intersatellite links, and missile tracking. In addition, both the millimeter and the submillimeter wave frequency spectra are required to detect most atmospheric constituents. The development of electronic components for the millimeter/submillimeter wave frequency spectrum is required for these applications.

For frequencies below 100 GHz, planar, quasi-TEM transmission lines such as microstrip and coplanar waveguide have been successfully used for monolithic amplifiers, mixers, and phase shifters. Although these planar, quasi-TEM type of transmission lines are highly suited for integrated circuits, the surface resistance increases with the square root of frequency [1]. In addition, the circuit dimensions must be decreased as the frequency is increased to maintain a single mode transmission line which further increases the conductor losses. The high attenuation makes microstrip and coplanar waveguide unsuitable for system integration or antenna feed networks in the millimeter and submillimeter wave frequency spectrum. Rectangular waveguide and other similar waveguides have low loss but are too large to effectively be used for many applications.

In recent years, a different class of transmission lines which do not require any conductors but instead use the difference in permittivities between two or more media to guide the electromagnetic energy have become popular. Examples of such dielectric waveguides are Image Guide [2], Insulated Image Guide [3], Trapped Image Guide [4], Dielectric Ridge Guide [5], Inverted Strip Dielectric Waveguide [6], and Layered Ridge Dielectric Waveguide (LRDW) [7]. These dielectric waveguides have been used in antenna feed networks, frequency scannable antennas, radars, and oscillators.

As the use of dielectric waveguides increases, better transitions between rectangular waveguide and the dielectric waveguide will be required for integrating the circuits with test equipment and millimeter wave sources such as Gunn diodes which typically have a rectangular waveguide output port. The transitions must match the impedances of the two waveguides and transform the TE_{10} mode of the rectangular waveguide to the propagating mode of the dielectric waveguide. The field

transformation is especially difficult since the fields are well confined in the rectangular waveguide but only weakly confined in the dielectric waveguide. As the permittivity of the dielectric waveguide is increased or multiple layers of dielectrics are used to reduce the size of the dielectric waveguide, the field transformation is more difficult to accomplish.

This paper will present an analysis of four transitions from rectangular waveguide to LRDW and a design procedure which could be followed to optimize the transition design. Both experimental as well as the Finite Difference Time Domain (FDTD) method will be used in the transition analysis. The design procedure is based on the concept of the Effective Dielectric Constant (EDC) method developed by McLevige [3]. Although the details of the analysis will be presented specifically for the LRDW, the methods and design procedures should be useful for other multi-layer dielectric waveguides as well.

II. Layered Ridge Dielectric Waveguide Description

Layered Ridge Dielectric Waveguide (LRDW) consists of a strip comprised of two or more layers of dielectrics on a conductor backed dielectric substrate. The center dielectric layer has a lower permittivity than the substrate and top layer. Fig. 1 shows the LRDW line with the dimensions and dielectrics used throughout this paper. Although the LRDW can support both E^x_{mn} and E^y_{mn} modes, the E^x_{11} mode has the lowest cutoff frequency and is therefore the dominant mode. Because of the continuity of the electric flux density across the dielectric boundaries for the E^x_{11} mode, the electric field is stronger in the low permittivity layer which becomes the guiding layer in the low frequency region of the spectrum.

To design a transition between a rectangular waveguide and an LRDW, the fields of both waveguides must be known in order to visualize the necessary field transformation which must occur. It has been shown that the EDC method is useful for obtaining an engineering estimate of the propagation constant and the fields for many dielectric waveguides [2]-[5]. Since the method has been fully presented in the literature, only a brief outline of it will be given here so that the important equations which will be required for this paper may be presented. The EDC method uses

the approximation that the LRDW may be separated and analyzed as two independent structures as shown in Fig. 2. Neither of these new structures has any variation along the y-axis and is therefore easier to solve. In general, the separation equation for Fig. 2 is given by:

$$k_z^2 = \epsilon_{ri} k_o^2 - k_{xi}^2 = \epsilon_{eq} k_o^2 \tag{1}$$

where $i = 1$ to N and N is the total number of dielectric layers, $k_o = \omega\sqrt{\epsilon_o \mu_o}$, k_{xi} is the separation variable for the $i\ th$ layer, and

$$\epsilon_{eq} = \epsilon_{ri} - \left(\frac{k_{xi}}{k_o}\right)^2 \tag{2}$$

is referred to as the effective dielectric constant for the region. Note that $k_{xN} = jh_x$ is commonly used since the fields in the $N\ th$ layer must be decaying to satisfy the radiation condition [1]. After ϵ_{eq} has been determined for each structure, the dielectric ridge can be replaced by the simple structure shown in Fig. 3. The separation equation for Fig. 3 is given by

$$k_z^2 = \epsilon_{eq}^I k_o^2 - k_{y1}^2 = \epsilon_{eq}^{II} k_o^2 + h_y^2 \tag{3}$$

which is used with the field equations to determine the propagation constant of the dielectric waveguide.

The fields for Fig. 2 may be written as a combination of LSM^x and LSE^x modes. Since the LSM^x mode is dominant over the portion of the frequency spectrum which results in strong field confinement within the guiding layer, it is sufficient to consider only the LSM^x mode in the analysis. Using these assumptions, the electric and magnetic fields for the structures shown in Fig. 2 may be written as:

$$H_{yi} = \omega \epsilon_o \epsilon_{ri} k_z \psi_i(x) \tag{4}$$

$$E_{xi} = (\epsilon_{ri} k_o^2 + \frac{\partial^2}{\partial x^2})\psi_i(x) \tag{5}$$

$$E_{zi} = -jk_z \frac{\partial \psi_i(x)}{\partial x} \tag{6}$$

For the four layer structure shown in Fig. 2(a), the scalar potential $\psi(x)$ may be written as:

$$\psi_1^I(x) = A_1 \cos(k_{x1}^I x), 0 < x < t_1 \tag{7}$$

$$\psi_2^I(x) = A_2\cos(k_{x2}^I(x-t_1)) + B_2\sin(k_{x2}^I(x-t_1)), t_1 < x < t_1+t_2 \quad (8)$$

$$\psi_3^I(x) = A_3\cos(k_{x3}^I(x-t_1-t_2)) + B_3\sin(k_{x3}^I(x-t_1-t_2)), t_1+t_2 < x < t_1+t_2+t_3 \quad (9)$$

$$\psi_4^I(x) = Ce^{-h_x^I(x-t_1-t_2-t_3)}, x > t_1+t_2+t_3 \quad (10)$$

After employing the boundary conditions at the dielectric interfaces, the eigenvalue equation is obtained as:

$$0 = (\frac{\epsilon_{r3}}{\epsilon_{r4}} - \frac{k_{x3}^I}{h_x^I}\tan(k_{x3}^I t_3))T^a + (\frac{k_{x3}^I}{h_x^I} + \frac{\epsilon_{r3}}{\epsilon_{r4}}\tan(k_{x3}^I t_3))T^b \quad (11)$$

$$T^a = \frac{\epsilon_{r1}}{\epsilon_{r3}} - \frac{\epsilon_{r2}}{\epsilon_{r3}}\frac{k_{x1}^I}{k_{x2}^I}\tan(k_{x1}^I t_1)\tan(k_{x2}^I t_2) \quad (12)$$

$$T^b = -\frac{\epsilon_{r1}}{\epsilon_{r2}}\frac{k_{x2}^I}{k_{x3}^I}\tan(k_{x2}^I t_2) - \frac{k_{x1}^I}{k_{x3}^I}\tan(k_{x1}^I t_1) \quad (13)$$

The parameters $k_{x1}^I, k_{x2}^I, k_{x3}^I$,and h_x^I are given from (1) as:

$$k_{x1}^I = k_o\sqrt{\epsilon_{r1} - \epsilon_{eq}^I} \quad (14)$$

$$k_{x2}^I = k_o\sqrt{\epsilon_{r2} - \epsilon_{eq}^I} \quad (15)$$

$$k_{x3}^I = k_o\sqrt{\epsilon_{r3} - \epsilon_{eq}^I} \quad (16)$$

$$h_x^I = k_o\sqrt{\epsilon_{eq}^I - 1} \quad (17)$$

The parameter h_x^I must be real, but the other parameters may be imaginary. Note that lossless dielectrics have been assumed. The eigenvalue equation, (11), is solved with (14)-(17) to obtain ϵ_{eq}^I. A similar set of equations is derived for the single layer structure shown in Fig. 2(b) to obtain the eigenvalue equation:

$$k_{x1}^{II}\tan(k_{x1}^{II}t_1) - \epsilon_{r1}h_x^{II} = 0 \quad (18)$$

with

$$k_{x1}^{II} = k_o\sqrt{\epsilon_{r1} - \epsilon_{eq}^{II}} \quad (19)$$

$$h_x^{II} = k_o\sqrt{\epsilon_{eq}^{II} - 1}$$

The structure of Fig. 3 can now be solved as a sum of LSE^y and LSM^y modes. Since the fields derived in the above analysis for Fig. 2 are primarily E_x and H_y, the LSM^y fields may be omitted.

The resulting fields are:

$$E_{xi} = -\omega\mu_o k_z \psi_i(y) \tag{20}$$

$$H_{yi} = (\epsilon_{eq}^{I,II} k_o^2 + \frac{\partial^2}{\partial y^2})\psi_i(y) \tag{21}$$

$$H_{zi} = -jk_z \frac{\partial \psi_i(y)}{\partial y} \tag{22}$$

where the scalar potentials are given by:

$$\psi_1(y) = A\cos(k_{y1}y), |y| < y_1 \tag{23}$$

$$\psi_2(y) = Be^{-h_y(|y|-y_1)}, |y| > y_1 \tag{24}$$

After satisfying the boundary conditions, the eigenvalue equation is obtained as:

$$k_{y1}\tan(k_{y1}y_1) - h_y = 0 \tag{25}$$

where

$$k_{y1} = k_o\sqrt{\epsilon_{eq}^I - \epsilon_{eff}} \tag{26}$$

$$h_y = k_o\sqrt{\epsilon_{eff} - \epsilon_{eq}^{II}}$$

and ϵ_{eff} is the effective dielectric constant for the LRDW.

III. Transition Description

In the past, three types of transitions from rectangular waveguide to dielectric waveguide have been commonly used. These are shown in Figs. 4(a)-(c). In the first transition shown in Fig. 4(a), referred to as transition A in the rest of the paper, the dielectric waveguide is abruptly butted to the full height rectangular waveguide [8]. For larger dielectric waveguides such as Image Guide fabricated from low permittivity materials, this transition can give good results since the size of the Image Guide is comparable to the size of the rectangular waveguide. The second transition shown in Fig. 4(b) will be referred to as transition B in the rest of the paper. In transition B, the rectangular waveguide is transitioned to a reduced height rectangular waveguide so that there is greater field interaction between the rectangular waveguide and the dielectric waveguide. The

rectangular waveguide may be made to be the same height as the dielectric waveguide but in practice, this is usually not done to allow for variations in the height of the dielectric waveguides. The most commonly used transition is shown in Fig. 4(c) and will be referred to as transition C in the rest of the paper. This transition adds a horn to transition B to convert the open dielectric waveguide to a shielded dielectric waveguide [9][10]. A forth transition shown in Fig. 4(d), referred to as transition D in the rest of the paper, uses a tapered ridge waveguide to concentrate the power of the rectangular waveguide to the region of the dielectric waveguide. The ridge is then continued into the horn to provide a smooth match to the open dielectric waveguide [11][12]. The ridge may be made to contact the dielectric waveguide. In each of these transitions, a dielectric wedge may be used to create the field transformation [13] or to improve the impedance match of the transition [14]. When the dielectric wedge is used for providing the field transformation, it must be 3-5 λ_g long.

As previously stated, it is critical to transform the electric and magnetic fields of the rectangular waveguide to the dielectric waveguide. The electric field magnitude, E_x, along the ground plane for each of the transitions at several cross sections is shown in Fig. 5. Note that transitions A and B have the same E_x field distribution. The EDC method has been used to determine the fields for the cross sectional cuts through the dielectric waveguide. The derivation outlined in section II was modified to account for the change in boundary conditions when the LRDW is in a shielded environment. The TE_{10} mode was assumed to exist in the rectangular waveguide. The fields in the ridge waveguide were determined from equations taken from [15] using the cutoff frequency determined by Hoefer [16].

From the field diagrams, it is noted that the horn on transitions C and D helps to transition the open dielectric waveguide to a shielded dielectric waveguide. No variation in the fields was seen for the LRDW at the end of the horn and the open LRDW. The ridge waveguide concentrates the electromagnetic energy in the region of the LRDW better than the other transitions. Furthermore, transition D transitions the rectangular waveguide fields to the LRDW fields more smoothly. Lastly, if only the dominant term of the electric field for the ridge waveguide is used, the ridge

waveguide and the shielded LRDW have the same E_x field distribution along the y-axis.

IV. Transition Analysis Using Finite Difference Time Domain

The FDTD method is well known [17] and thus will not be presented here. The excitation mechanism used in this research is similar to that described in [18],[19]. To approximate the TE_{10} mode, the amplitude of the incident field has a half wavelength sinusoidal distribution across the rectangular guide in the y-direction and is uniform in the x-direction. Moreover, the incident field has a spatial variation in the z-direction given by a Gaussian envelope imposed on a sinusoidally varying carrier. The super-absorbing first-order Mur boundary condition [20] is used at the front and back walls of the computational domain in order to simulate infinitely long lines. Numerical experiments have shown that such an absorbing boundary condition (ABC) reduces reflections appreciably compared to, for example, first-order Mur without the super-absorber [14]. The above ABC's require a choice for the incident velocity of the waves, or equivalently ϵ_{eff}. At the front wall, an ϵ_{eff} that corresponds to the velocity of the waves in an empty waveguide, at a frequency which is approximately at the middle of the frequency range of interest, is chosen. On the other hand, at the back wall, an ϵ_{eff} that corresponds to the velocity of the waves in the LRDW is chosen. An estimate of this latter ϵ_{eff} may be obtained using the compact 2D-FDTD technique [21][22] or the mode matching technique [7]. It should be mentioned that the above choice of ϵ_{eff} assumes that only the propagating dominant mode exists in the dielectric waveguide. The first-order Mur boundary condition was used on the top and side walls surrounding the LRDW in order to simulate an open structure.

V. Experimental Characterization of Transitions

The LRDW was fabricated from RT/Duroid^{TM} 5880 and 6010 substrates which have relative permittivities of 2.2 and 10.8 respectively. Rogers^{TM} 3001 bonding film was used to glue the substrates together. The transitions were characterized using an HP8510B Vector Network Analyzer with a WR-28 Reflection/Transmission test set. The system was calibrated using an open-short-

load calibration procedure. For the through measurements, two transitions were connected back to back through a 19 cm long section of LRDW. The same LRDW was used for all of the measurements so that comparisons between transitions could be made. For the return loss measurements, microwave absorbing material was placed over the LRDW to eliminate power returned from the second transition. Before each set of data was taken, the time domain option of the HP8510 was used to verify that all of the reflections were due to the transitions and not because of fabrication imperfections in the LRDW. To fabricate the dielectric wedges, RT/Duroid^{TM} 5880, 6010, and 6006 which has a dielectric constant of 6.0 were used. Standard microwave substrate thicknesses in the range of 0.0254 to 0.157 cm were used.

VI. Transition Analysis Using TLIN Method

The analysis of many microwave circuit problems may be greatly simplified through the use of Transmission Line Theory (TLIN) and wave impedances. In general, wave impedances are defined as the ratio of the transverse field components which give rise to power flow along a mutually perpendicular axis. For Transverse Electric modes, the wave impedance may be written in the general form:

$$Z = \frac{k_o \eta_o}{k_z} \tag{27}$$

which translates to:

$$Z = \frac{\eta_o}{\sqrt{\epsilon_{eff} - (\lambda_o/\lambda_c)^2}} \tag{28}$$

for perfectly conducting cylindrical waveguides and to:

$$Z = \frac{\eta_o}{\sqrt{\epsilon_{eff}}} \tag{29}$$

for open dielectric waveguides. The parameters in (27)-(29) are: $\eta_o = \sqrt{\mu_o/\epsilon_o}$ is the free space impedance, λ_o is the free space wavelength, ϵ_{eff} is the effective permittivity of the medium filling the waveguide, and λ_c is the cutoff wavelength of the empty cylindrical waveguide.

Although it is possible to take a large number of cross sectional cuts through the transition, determine the wave impedance at each plane, and calculate the reflection coefficient very accurately, a good engineering estimate of the reflection coefficient may be obtained if only the most

significant impedance mismatches are used. Fig. 6 shows a time domain plot of S_{11} for transition D measured on the HP8510B. The markers are positioned at three reflection points along the transition. Marker 1 is at the start of the LRDW under the ridge, Marker 2 is at a point inside the horn, and Marker 3 is at the end of the horn. It is clear that the reflection from the start of the LRDW is far larger than any other reflection and for an engineering estimate of the reflection coefficient for the transition, all other parts of the transition may be omitted. Using these assumptions, the transitions may be analyzed using the TLIN method at the single discontinuity which results in the simple equation:

$$\Gamma = \frac{Z^w - Z^d}{Z^w + Z^d} \tag{30}$$

where Z^w is the wave impedance of the rectangular or ridged waveguide and Z^d is the wave impedance of the open or shielded dielectric waveguide. The ϵ_{eff} of the dielectric guides and the partially filled rectangular waveguides were determined from the EDC method. The cutoff wavelengths of the ridge waveguides were calculated using Hoefer's equations [16].

VII. Results

The fields of the open LRDW at 33 GHz determined by both the EDC and the 2D-FDTD methods are shown in Figs. 7 and 8. Excellent agreement between the two methods is seen for the fields plotted along the x-axis, Fig. 7. This is expected since a magnetic wall exists along the x-axis for the mode plotted which has the effect of eliminating the contributions of the ridge edges from the analysis. The magnitude of the fields not shown were either zero or very small compared to those presented. The difference in the fields shown in Fig. 8 is greater than that of Fig. 7. This is a direct result of the edge contributions not adequately being accounted for in the EDC method. Although the magnitudes of the fields in Fig. 8 are not in good agreement, the field shape is in good agreement. Note that the power shown in Fig. 7(d) is confined in the low permittivity layer or the guiding layer.

To verify the accuracy of the TLIN and the FDTD methods of analysis, $|S_{11}|$ has been plotted for all of the transitions in Fig. 9. Several observations are made. First, the measured return

loss is lower than that predicted by the TLIN and the FDTD methods. This is expected since the FDTD method does not take into account the conductor and dielectric losses, whereas the TLIN method assumes a completely lossless junction. Second, except for transition A, the agreement between the theoretically predicted loss (using the TLIN and the FDTD) and the measured return loss is satisfactory. In each case, the three methods yield a return loss within ± 3 dB of each other. Furthermore, the TLIN method and the FDTD method are generally within ± 1.5 dB of each other. The FDTD analysis was not performed for transition A. Also, for transition A, the TLIN method is not in agreement with the measurements because of the small field overlap between the two waveguides which makes the TLIN method less accurate. Third, the FDTD method accurately predicts the general shape of S_{11}, even predicting the presence of the major resonances.

Fig. 10 shows the measured insertion loss for transitions A, C, and D. The insertion loss of transitions B and C is approximately the same across the band with the exception of the higher frequency part of the band when a resonance is noted in transition C. Transition A has a greater insertion loss than the other transitions and the insertion loss of transition D is at least 2 dB less than the other transitions. When the loss factor, $1 - |S_{11}|^2 - |S_{21}|^2$, is calculated for each of the transitions, it is noted that transition D has the lowest loss factor while transition A has the greatest loss factor. Since ridge waveguide has higher conductor loss than rectangular waveguide, it follows that transition D has the lowest radiation loss of the four transitions; at least 1 dB per transition lower than transition C. This result was expected from the better field match of transition D as noted in Fig. 5. Also, it may be stated that minimizing the return loss alone is not a valid design criteria for open transitions. Although transitions A and C had the lowest measured return loss, they also had the highest radiation loss which makes them undesirable for transitions to antenna feed networks or other applications where crosstalk must be minimized.

Resonances in the insertion loss plots for transitions C and D at the higher frequencies are seen in Fig. 10. By correlating the onset frequency of the resonances with the cutoff frequencies of the higher order rectangular waveguide modes in the horn and with the field plots for both the

LRDW and the rectangular waveguide, it has been determined that the resonances are due to the TE_{31} mode in the rectangular horn. Reducing the width of the horn shifts the onset frequency of the resonances to higher frequencies and may be used to eliminate them from the waveguide band. A slight degradation in S_{11} would be expected if this were done. Note the 2-3 dB degradation in $|S_{11}|$ between Fig. 9 (b) which has no horn and Fig 9 (c) which has a horn.

To provide impedance matching between the rectangular waveguide and the LRDW, dielectric wedges were added to the transitions. For Image Guide and other single material dielectric waveguides, the dielectric wedges are typically constructed from the same material as the guiding layer of the dielectric waveguide [13][14]. For layered dielectric waveguides, this is not practical. To determine the optimum wedge material, thickness, and length for the LRDW, the characteristics of each transition was experimentally characterized for many matching wedges. It was determined that for transitions B, C, and D, a dielectric wedge with a relative permittivity of 6.0, a thickness of 0.127 cm, and a length of 1.91 cm provided optimum return loss. Although longer wedges tended to reduce the return loss, they also created resonances in the $|S_{21}|$ characteristics due to reflections between the two ends of the wedge. This was easily seen using the time domain option of the HP8510B ANA.

The use of the matching wedge greatly improved the measured characteristics of each transition. Fig. 11 shows the measured as well as the calculated return loss and the measured insertion loss of transition D with the experimentally determined optimum matching wedge. Note that the return loss is typically 20 dB compared to the 14 dB without the wedge. Also, the high frequency noise seen on the insertion loss plots of Fig. 10 have been eliminated. Table 1 summarizes the measured performance of each transition. In Table 1, the worst case return loss value across the waveguide band is given. Transition D has the lowest insertion loss and the best return loss. Also, there is a significant improvement in the characteristics of transitions B and C with the addition of the dielectric wedge. In these two transitions, the dielectric wedge not only provides impedance matching but is also the only means of transforming the fields of the two different waveguides.

To gain a better understanding of the transition, the FDTD method was used to obtain electric

field along the center of the waveguide for transitions C and D without a matching wedge. These are shown in Figs 12 (a) and (b) respectively. The transmitted wave is approximately at the same location in each figure. Notice that the power transitioned to the LRDW is confined in the low dielectric layer. Furthermore, this guided signal in the LRDW lags the radiated power emerging from the horn as expected. The radiated power is especially evident in Fig. 12 (a) where the plane wave emerging from the horn is easily seen. Comparing the two figures, it is seen that transition D has a smaller radiated signal than transition C. In fact, although the pulse in Fig. 12 (b) is slightly ahead of the pulse in Fig. 12 (a), no radiated plane wave is apparent.

VIII. Design Guidelines

The data presented shows the advantage of using a flared horn on the output of the transition to better match the shielded LRDW to the open LRDW. The data has also shown that the width of the horn must be controlled to eliminate the TE_{31} mode which couples to the LRDW and creates resonances. Furthermore, it has been shown that a dielectric wedge may be used to greatly improve the return loss characteristics of the transitions. Lastly, it has been shown in Figs. 9 and 11 that the EDC method can accurately be used to calculate the return loss of the transitions. It is therefore reasonable to use the EDC method as a design aid.

In this section the EDC method will be used to optimize the dielectric matching wedge parameters. From TLIN theory, the return loss is minimized when the wave impedances of the two waveguides are equal. For transitions A and B where the LRDW is unshielded, this translates to the condition:

$$\frac{\eta_o}{\sqrt{\epsilon^{LRDW}}} = \frac{\eta_o}{\sqrt{\epsilon^w - (\lambda_o/\lambda_c^w)^2}} \tag{31}$$

and for transitions C and D where the LRDW is shielded the matching condition is:

$$\frac{\eta_o}{\sqrt{\epsilon^{LRDW} - (\lambda_o/\lambda_c^{LRDW})^2}} = \frac{\eta_o}{\sqrt{\epsilon^w - (\lambda_o/\lambda_c^w)^2}} \tag{32}$$

where ϵ^{LRDW} is the effective dielectric constant of the LRDW, ϵ^w is the effective dielectric constant of the partially filled rectangular waveguide or ridged waveguide containing the dielectric matching wedge, and λ_c^{LRDW} and λ_c^w are the cutoff wavelengths of the empty rectangular waveguide or

ridged waveguide housing the LRDW and the dielectric wedge respectively. (31) and (32) may be simplified to:

$$\epsilon^w = \epsilon^{LRDW} + (\lambda_o/\lambda_c^w)^2 \tag{33}$$

and

$$\epsilon^w = \epsilon^{LRDW} - (\lambda_o/\lambda_c^{LRDW})^2 + (\lambda_o/\lambda_c^w)^2 \tag{34}$$

respectively. If the LRDW is in the same waveguide as the dielectric wedge, then $\lambda_c^{LRDW} = \lambda_c^w$ and (34) simply states that the effective permittivities of the two waveguides must be matched. Since all of the terms on the right hand side of (33) and (34) are known, ϵ^wmay be determined.

The design will proceed for transitions C and D although the relevant equations may be replaced to optimize transitions A and B. Start with the eigenvalue equation for the determination of the parameter k_y (analogous to (25)). For the LRDW in the transition, a magnetic wall exists along the x-axis and an electric wall at y_2 must be used to represent the side walls of the rectangular waveguide. The resulting equation is:

$$k_{y1}\tan(k_{y1}y_1) - k_{y2}\cot(k_{y2}(y_2 - y_1)) = 0 \tag{35}$$

where:

$$\begin{aligned} k_{y1} &= k_o\sqrt{\epsilon_{eq}^I - \epsilon^w} \\ k_{y2} &= k_o\sqrt{1 - \epsilon^w} \end{aligned} \tag{36}$$

and ϵ_{eq}^I is the equivalent dielectric constant for the region of the guide containing the dielectric wedge and y_1 is equal to one half of the wedge width. In (36), the assumption that $\epsilon_{eq}^{II} = 1$ was used. For most cases, this is valid since the substrate is generally very thin to suppress surface wave modes which would cause power leakage. ϵ_{eq}^I may be obtained through the solution of (35) with (36) and the assumption that the width of the wedge and the LRDW are equal.

Knowing ϵ_{eq}^I, it is possible to solve for the permittivity of the dielectric wedge, ϵ_{r1}, as a function of the wedge thickness, t_1, using the eigenvalue equation for the parameter k_x. For the case of two dielectric regions bound by perfect conductors, the eigenvalue equation is:

$$\frac{k_{x1}}{\epsilon_{r1}}\tan(k_{x1}t_1) + k_{x2}\tan(k_{x2}(x_2 - t_1)) = 0 \tag{37}$$

where:

$$k_{x1} = k_o\sqrt{\epsilon_{r1}^I - \epsilon_{eq}^I} \tag{38}$$
$$k_{x2} = k_o\sqrt{1 - \epsilon_{eq}^I}$$

and x_2 is the total height of the shield.

The solution of (37) and (38) results in a set of permittivities and thicknesses for the dielectric wedge which are each optimized according to the TLIN method. The task now is to choose the optimum combination from this set of solutions. The equalization of wave impedances is not sufficient if there is little field overlap between the two waveguides. This was seen in Fig. 9 (a) which is the return loss for transition A. It is also necessary to optimize the field match between the two waveguides. This can be accomplished through a mode matching analysis [23]. If the analysis is simplified to use only the dominant mode in each waveguide, the reflection coefficient is given by:

$$\Gamma = \frac{I_{11}I'_{11} - I_1 I'_1}{I_{11}I'_{11} + I_1 I'_1} \tag{39}$$

where:

$$I_1 = \int_0^a (E^w(x))^2 dx \tag{40}$$
$$I'_1 = \int_0^{a'} (H^{LRDW}(x))^2 dx$$
$$I_{11} = \int_0^a E^w(x) E^{LRDW}(x) dx$$
$$I'_{11} = \int_0^{a'} H^w(x) H^{LRDW}(x) dx$$

and a and a' are the height of the two waveguides. The field components can be obtained from the EDC analysis. As a further simplification, the fields are taken for the case equivalent to Fig. 2 (a). This is justified since most of the energy is confined at the center of the LRDW, the center of the ridge waveguide, and the center of the reduced height rectangular waveguide when the dielectric wedge is present. It is a simple procedure to solve (39) for each of the possible wedge combinations obtained from the TLIN analysis.

When this procedure was performed for the transitions C and D, it was found that the optimum

wedge parameters are $\epsilon_r = 7.0$ with a thickness of 0.107 cm and $\epsilon_r = 6.0$ with a thickness of 0.112 cm respectively. Note that this is very close to the optimum wedge parameters of $\epsilon_r = 6.0$ and a thickness of 0.127 cm found experimentally where only standard substrate permittivities and thicknesses could be used. Furthermore, the optimum wedge thickness corresponds to the thickness of the LRDW for the cases presented. Although this may not be true for all dielectric waveguides and for all frequencies, a first order design of the wedge may be obtained by using (33-38) with that assumption.

IX. Conclusions

Four transitions were analyzed using a transmission line (TLIN) analysis, a Finite Difference Time Domain Analysis (FDTD), and experimentally. It has been shown that the FDTD analysis accurately models the transitions. In addition, it was shown that the TLIN method gave acceptable results. Using the Effective Dielectric Constant and the TLIN methods, a simple design procedure was given for the transition design and the design of the dielectric matching wedge. For small sized dielectric waveguides such as LRDW, a transition comprised of a tapered ridge waveguide reduced the radiation loss of the transition by approximately 1 dB while simultaneously having an excellent return loss.

X. Acknowledgments

This work was supported by the Army Research Office (ARO) and the NASA Lewis Research Center Director's Discretionary Fund.

References

[1] R. E. Collin, *Foundation for Microwave Engineering*, McGraw-Hill Book Co., New York, 1966.

[2] R. M. Knox and P. P. Toulios, "Integrated circuits for the millimeter through the optical frequency range," *Proc. Symp. Submillimeter Waves*, pp. 497-516, New York, March 31-April 12, 1970 .

[3] W. V. McLevige, T. Itoh, and R. Mittra, "New waveguide structures for millimeter-wave and optical integrated circuits," *IEEE Trans. Microwave Theory Tech.*, pp. 788-794, Oct. 1975.

[4] T. Itoh and B. Adelseck, "Trapped image guide for millimeter-wave circuits," *IEEE Trans. Microwave Theory Tech.*, pp. 1433-1436, Dec. 1980 .

[5] T. Wang and S. E. Schwarz, "Design of dielectric ridge waveguides for millimeter-wave integrated circuits," *IEEE Trans. Microwave Theory Tech.*, pp. 128-134, Feb. 1983.

[6] T. Itoh, "Inverted strip dielectric waveguide for millimeter-wave integrated circuits," *IEEE Trans. Microwave Theory Tech.*, pp. 821-827, Nov. 1976.

[7] A. G. Engel, Jr. and L. P. B. Katehi, "Low-loss monolithic transmission lines for submillimeter and terahertz frequency applications," *IEEE Trans. Microwave Theory Tech.*, pp. 1847-1854, Nov. 1991.

[8] K. Solbach, "Electric probe measurements on dielectric image lines in the frequency range of 26-90 GHz," *IEEE Trans. Microwave Theory Tech.*, pp. 755-758, Oct. 1978.

[9] A. K. Tiwari and R. P. Singh, "An efficient image guide mode launcher," *Int. Journal of Infrared and Millimeter Waves*, Vol. 7, No. 6, pp. 845-856, 1986.

[10] M. Dydyk, "Image guide: a promising medium for EHF circuits," *Microwaves*, pp. 71-80, April 1981.

[11] T. H. Oxley and P. L. Lowbridge, "Image guide and microstrip integrated W-band receivers," *Microwave Journal*, pp. 117-136, Nov. 1983.

[12] G. E. Ponchak, N. I. Dib, and L. P. B. Katehi, "A novel transition between rectangular waveguide and layered ridge dielectric waveguide," *Proc. 24th European Microwave Conf.*, Cannes, France, pp. 1933-1937, Sept. 5-8, 1994.

[13] S. A. Pogarsky and I. I. Saprykin, "Resonant phenomena in hybrid structures," *Int. Journal of Infrared and Millimeter Waves*, Vol. 15, No. 7, pp. 1325-1333, 1994.

[14] N. I. Dib and L. P. B. Katehi, "Analysis of the transition from rectangular waveguide to shielded dielectric image guide using the finite-difference time-domain method," *IEEE Microwave and Guided Wave Letters*, pp. 327-329, Sept. 1993.

[15] W. J. Getsinger, "Ridge waveguide field description and application to directional couplers," *IRE Trans. Microwave Theory Tech.*, pp. 41-50, Jan. 1962.

[16] W. J. R. Hoefer and M. N. Burton, "Closed-form expressions for the parameters of finned and ridged waveguides," *IEEE Trans. Microwave Theory Tech.*, pp. 2190-2194, Dec. 1982.

[17] K. Kunz and R. Luebbers, *The Finite Difference Time Domain Method for Electromagnetics, Florida*: CRC press, 1993.

[18] P. Alinikula and K. Kunz, "Analysis of Waveguide Aperture Coupling Using the Finite-Difference Time-Domain Method, " *IEEE Microwave Guided Wave Lett.*, vol. 1, pp. 189-191, Aug. 1991.

[19] M. De Pourcq, "Field and Power-Density Calculations in Closed Microwave Systems by Three-Dimensional Finite Differences, " *IEE Proc.*, vol. 132, Pt. H, no. 6, pp. 360-368, October 1985.

[20] K. Mei and J. Fang, "Superabsorption- A Method to Improve Absorbing Boundary Conditions, " *IEEE Trans. Antennas and Propagation*, vol. 40, pp. 1001-1010, Sept. 1992.

[21] A. Asi and L. Shafai, "Dispersion Analysis of Anisotropic Inhomogeneous Waveguides Using Compact 2D-FDTD, " *Electronics Letters*, vol. 28, no. 15, pp. 1451-1452, July 1992.

[22] N. Dib and L. Katehi, "Dispersion Analysis of Multilayer Planar Lines Containing Ferrite Regions Using an Extended 2D-FDTD Method, " *1993 AP-S Symposium Digest*, pp. 842-845, Ann Arbor, Michigan, June 1993.

[23] D. M. Pozar, *Microwave Engineering*, Addison-Wesley Publishing Co., New York, 1990.

Table 1.—Summary of measured transitions performance.

Transition type	S_{11} (dB)	S_{21} at 26.5 GHz (dB)	S_{21} at 40.0 GHz (dB)
A, no wedge	12.8	5.0	18.0
B, no wedge	10.2	9.0	12.0
B, with wedge	12.3	5.5	10.0
C, no wedge	11.6	8.0	13.0
C, with wedge	16.0	4.8	10.5
D, no wedge	12.3	5.5	10.0
D, with wedge	16.2	5.5	8.2

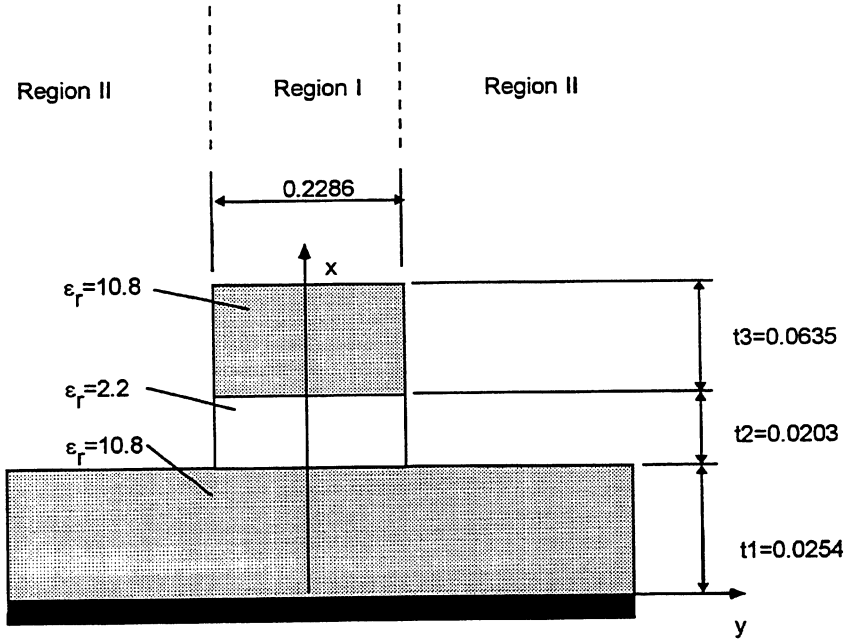

Figure 1.—Layered ridge dielectric waveguide for 26.5-40 GHz (dimensions in cm).

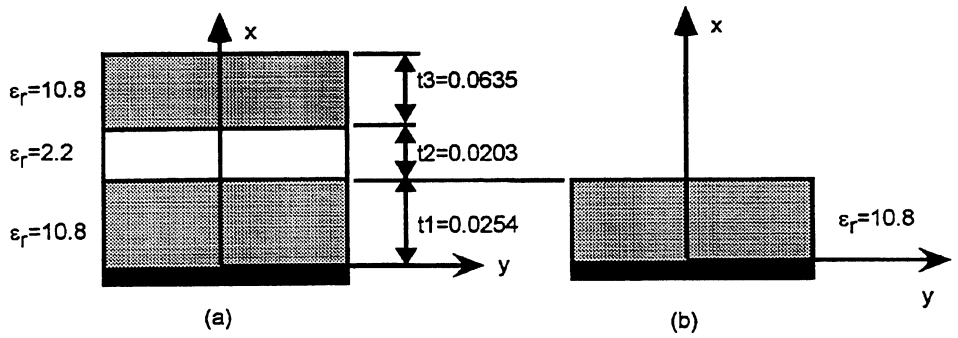

Figure 2.—Structures for analyzing the parameter k_x using the EDC method where (a) represents region I and (b) represents region II.

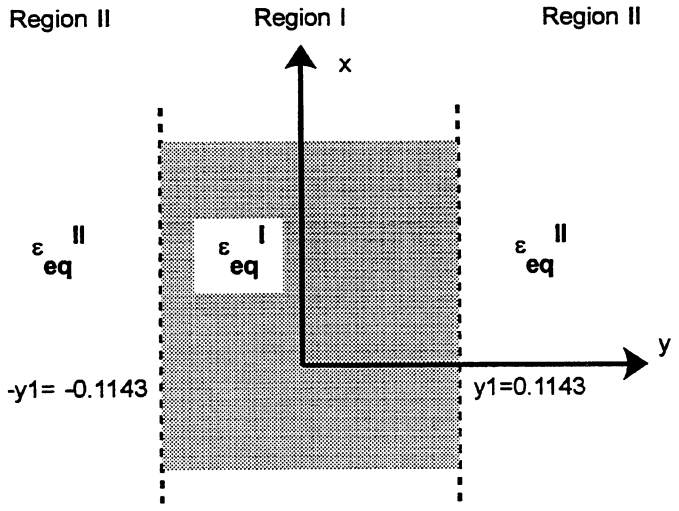

Figure 3.—Structure for analyzing the parameter k_y using the EDC method.

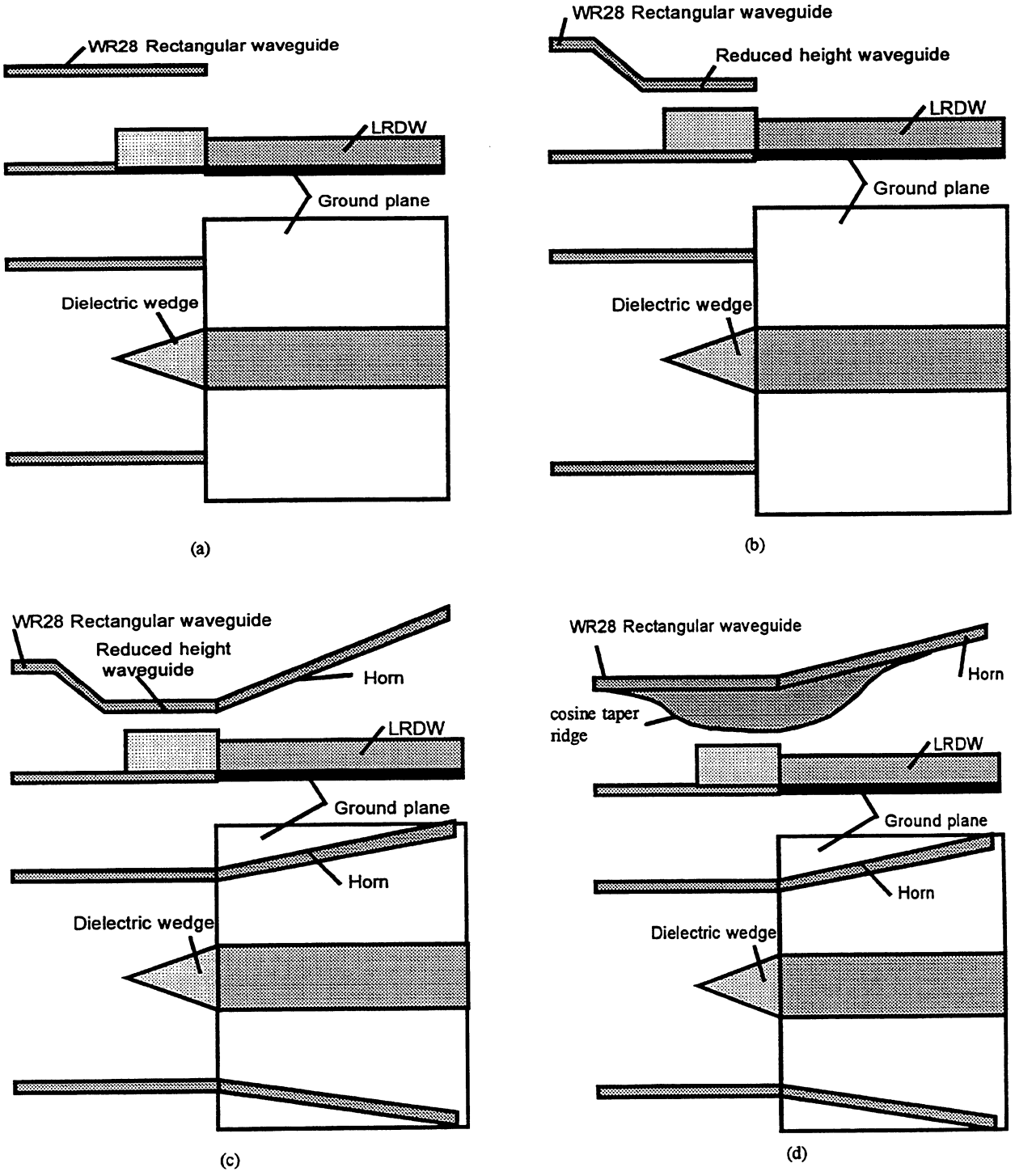

Figure 4.—Transitions from rectangular waveguide to layered ridge dielectric waveguide where (a), (b), (c), and (d) shows transitions A, B, C, and D respectively.

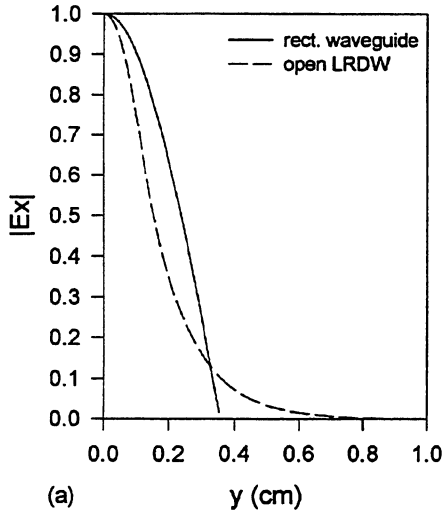

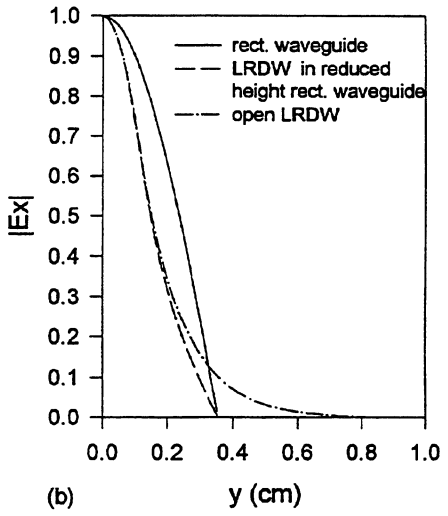

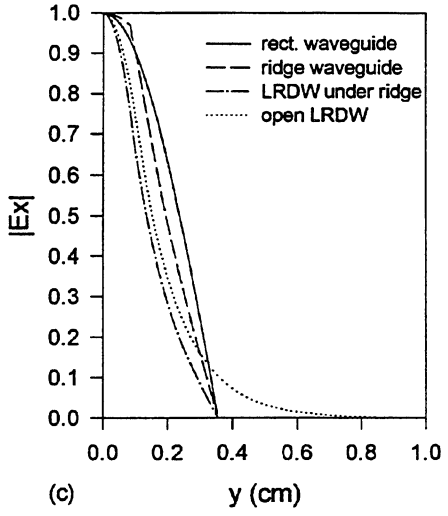

Figure 5.—$|E_x|$ at x = 0 for cross sectional cuts through transitions A and B in (a), transition C in (b) and transition D in (c).

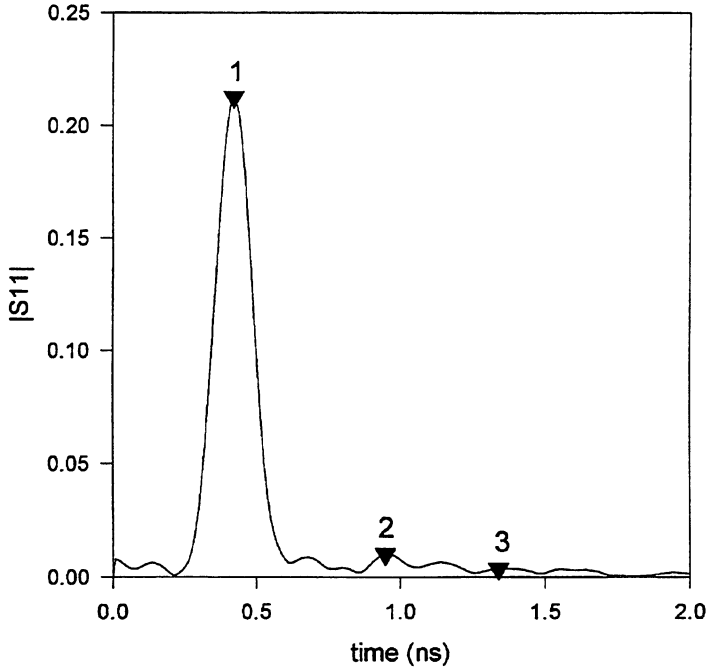

Figure 6.—Measured time domain S_{11} for transition D with no matching wedge.

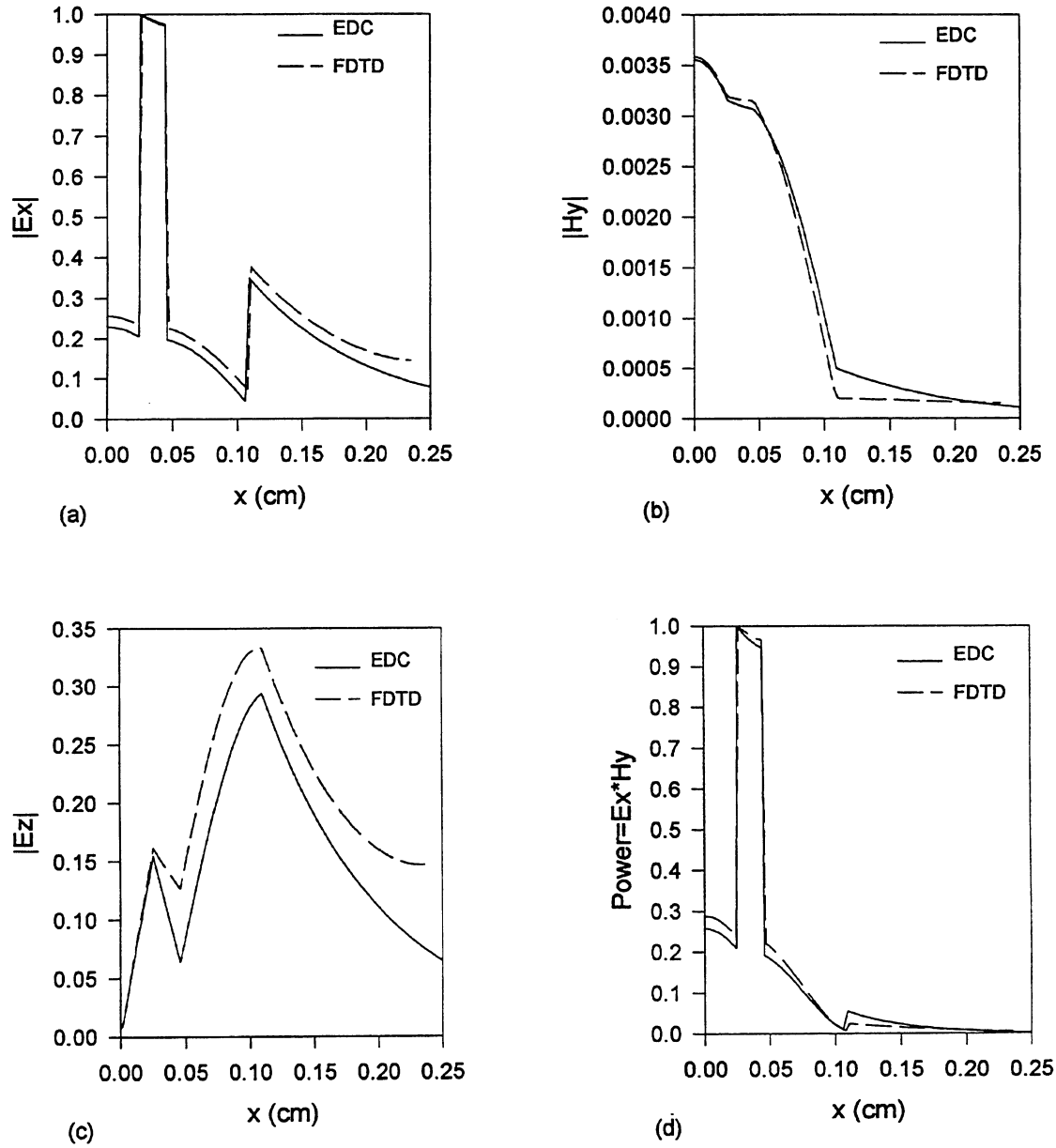

Figure 7.—Electric and magnetic field magnitudes along the x-axis of the LRDW at 33 GHz determined by the EDC and the FDTD methods.

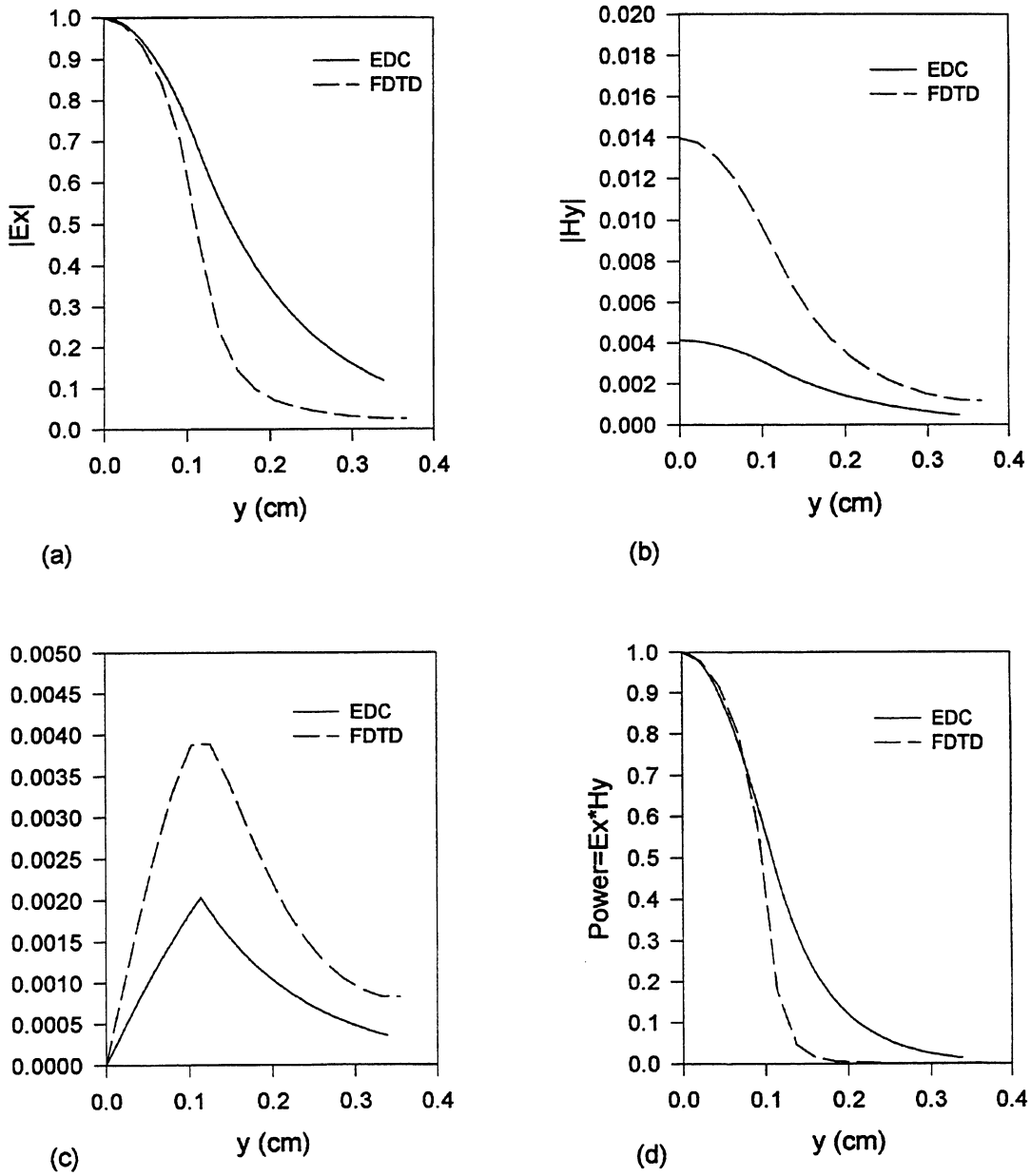

Figure 8.—Electric and magnetic field magnitudes along the y-axis of the LRDW at 33 GHz determined by the EDC and the FDTD methods.

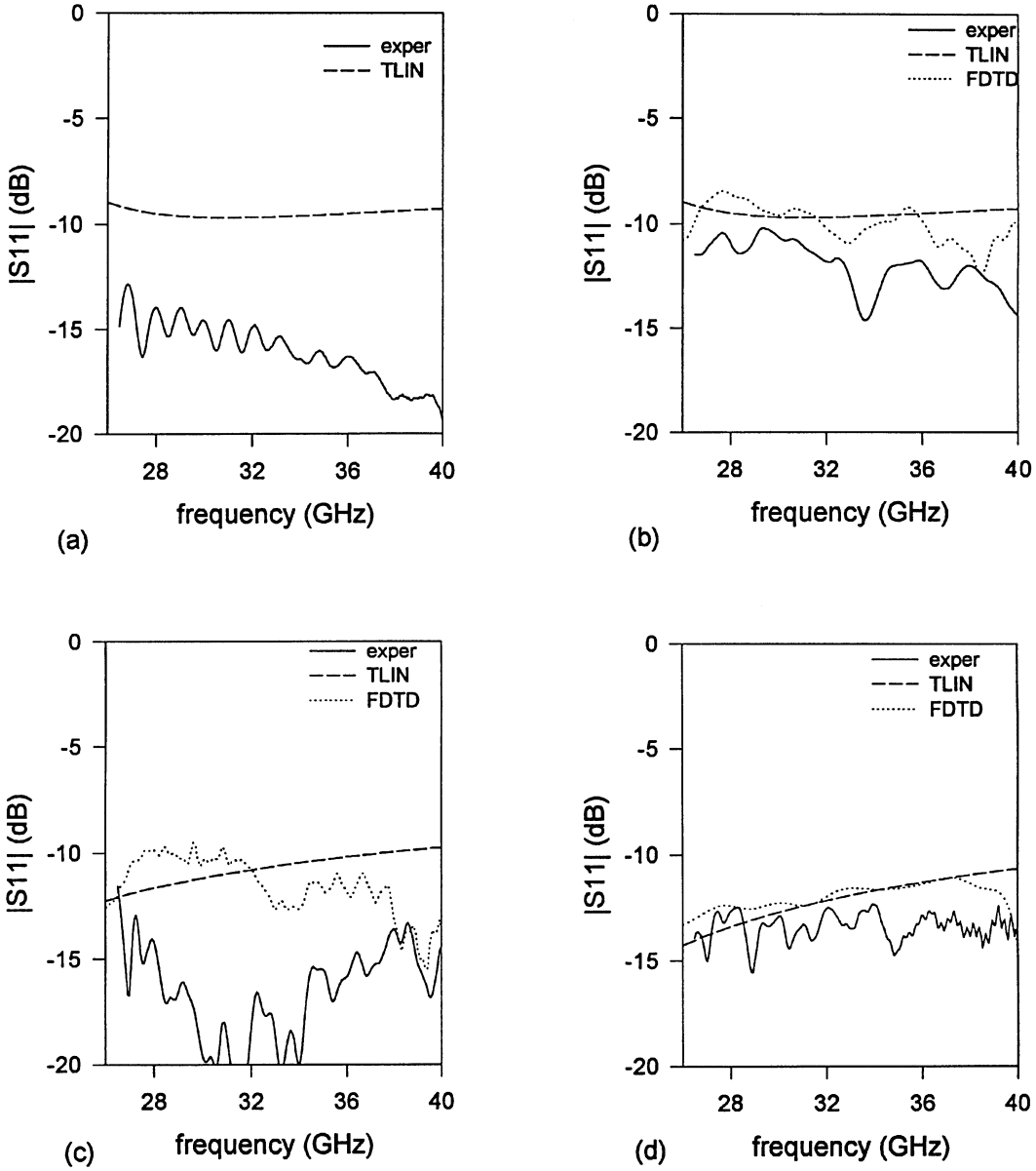

Figure 9.—Measured and calculated return loss for transitions A, B, C, and D in (a), (b), (c), and (d) respectively.

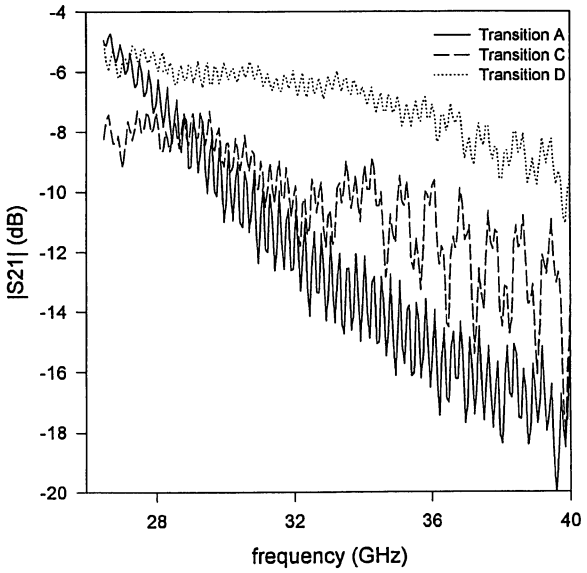

Figure 10.—Measured insertion loss of transitions A, C, and D without a dielectric matching wedge.

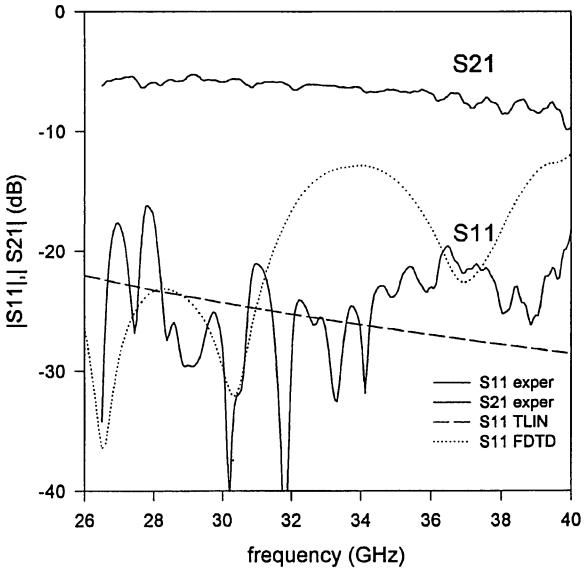

Figure 11.—Measured and calculated characteristics of transition D with a dielectric matching wedge.

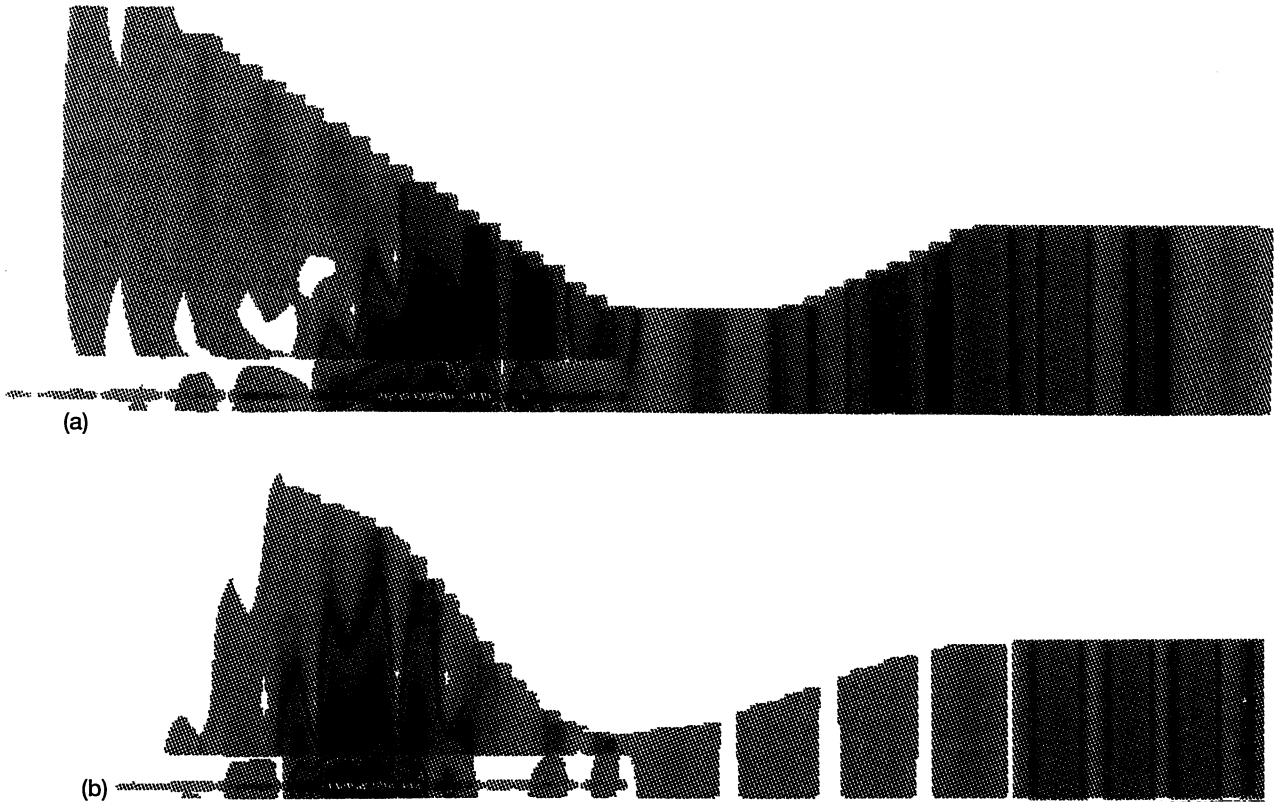

Figure 12.—Electric field along the center of the waveguide at 33 GHz without a dielectric wedge calculated using FDTD method. Transition C in (a) and transition D in (b).

REPORT DOCUMENTATION PAGE

Form Approved
OMB No. 0704-0188

1. AGENCY USE ONLY (*Leave blank*)	2. REPORT DATE	3. REPORT TYPE AND DATES COVERED
	March 1996	Technical Memorandum

4. TITLE AND SUBTITLE
Design and Analysis of Transitions from Rectangular Waveguide to Layered Ridge Dielectric Waveguide

5. FUNDING NUMBERS
WU-233-5A-5A

6. AUTHOR(S)
George E. Ponchak, Nihad I. Dib, and Linda P.B. Katehi

7. PERFORMING ORGANIZATION NAME(S) AND ADDRESS(ES)
National Aeronautics and Space Administration
Lewis Research Center
Cleveland, Ohio 44135-3191

8. PERFORMING ORGANIZATION REPORT NUMBER
E-10126

9. SPONSORING/MONITORING AGENCY NAME(S) AND ADDRESS(ES)
National Aeronautics and Space Administration
Washington, D.C. 20546-0001

10. SPONSORING/MONITORING AGENCY REPORT NUMBER
NASA TM-107173

11. SUPPLEMENTARY NOTES
George E. Ponchak, NASA Lewis Research Center; Nihad I. Dib, Jordan University of Science and Technology, Jordan; Linda P.B. Katehi, University of Michigan, Ann Arbor, Michigan. Responsible person, George E. Ponchak, organization code 5620, (216) 433-3504.

12a. DISTRIBUTION/AVAILABILITY STATEMENT
Unclassified - Unlimited
Subject Category 17

This publication is available from the NASA Center for Aerospace Information, (301) 621-0390.

12b. DISTRIBUTION CODE

13. ABSTRACT (*Maximum 200 words*)

Transitions from rectangular waveguide to layered ridge dielectric waveguide are studied both experimentally and theoretically. In addition, a design procedure is given for each transition. The analysis and design procedures are valid for transitions between rectangular waveguide and other open dielectric waveguides such as Image Guide, Insulated Image Guide, Dielectric Ridge Guide, and Inverted Strip Dielectric Waveguide. It is shown that for small dielectric waveguides such as a Layered Ridge Dielectric Waveguide, a transition which is comprised of a tapered ridge waveguide reduces the radiation loss by at least 1 dB.

14. SUBJECT TERMS	15. NUMBER OF PAGES
Millimeter wave; Microwave; Transmission lines; Waveguides; Transitions	28
	16. PRICE CODE: A03

17. SECURITY CLASSIFICATION OF REPORT	18. SECURITY CLASSIFICATION OF THIS PAGE	19. SECURITY CLASSIFICATION OF ABSTRACT	20. LIMITATION OF ABSTRACT
Unclassified	Unclassified	Unclassified	

National Aeronautics and
Space Administration

Lewis Research Center
21000 Brookpark Rd.
Cleveland, OH 44135-3191